Article

Long-duration Catalytic Steam Reforming of 2nd Generation Bio-Ethanol

Zehao Li [1,†], Yilu Wu [1,†], Miao Yang [2], Jan Baeyens [3], Shuo Li [1,*], and Huili Zhang [1,*]

[1] College of Life Science and Technology, Beijing University of Chemical Technology, Beijing 100029, China
[2] Beijing Advanced Innovation Center for Soft Matter Science and Engineering, Beijing University of Chemical Technology, Beijing 100029, China
[3] Department of Chemical Engineering, KU Leuven, 3001 Leuven, Belgium
* Correspondence: ssure@163.com (S.L.); zhhl@buct.edu.cn (H.Z.)
† These authors contributed equally to this work.
Received: 12 August 2025; Revised: 28 August 2025; Accepted: 4 September 2025; Published: 8 September 2025

Abstract: Hydrogen can be produced by catalytically steam-converting bio-ethanol (CSRE). The present research applies EtOH from fermenting pretreated biomass (second-generation process). The endothermic CSRE reaction is operated at moderate temperatures (450 to 600 °C). Non-noble bi-metallic catalysts are applied: mostly Co, doped with minor promoting Ce amounts, were used as active species and wet-impregnated on α-Al_2O_3. The catalyst and its supports were fully characterized. Between 450 and 600 °C, in different experimental setups, mainly H_2 and CO_2 are formed at high molar steam to ethanol ratio. Yields of 5 to 5.72 mol H_2/mol EtOH, and up to 1.84 mol CO_2/mol EtOH, are obtained respectively. Both CO and CH_4 were detected at very low concentrations. The Co/α-Al_2O_3 and Co-Ce/α-Al_2O_3 catalysts are very stable and not deactivated during long-duration testing of 2000 h while previous literature is limited to less than 30 h. A solar pilot-scale bio-ethanol CSRE using a particle-driven thermal loop was also tested and is reported to produce 5 mol H_2/ mol EtOH at the low 480 ± 20 °C. Experiments are ongoing at 550 to 600 °C.

Keywords: 2nd generation bio-ethanol; catalytic reforming; steam; hydrogen; pilot scale; hot particle loop

1. Introduction

1.1. Ethanol Conversion by Catalytic Steam Reforming

The development and production of "green" H_2, i.e., produced from "green" feedstock material and using renewable energy as its driving energy source, attracts an increasing research and industrial attention. Methanol and ethanol are recognized as suitable feedstock among the available oxygenated fuels [1,2]. Ethanol has however the advantage over methanol by being a cheaper, non-toxic, and available biomass-based feedstock derived through either first- or second-generation fermentation principles [3–5]. The majority of ethanol remains fossil-based synthesized.

Within the reported thermal ethanol to H_2 methods, the catalytic steam-ethanol conversion has merits of a high hydrogen yield, high reaction rates and fair required heat of reaction, as presented in (R1) below:

$$C_2H_5OH + 3H_2O \rightarrow 6H_2 + 2CO_2 \; \Delta H^0_{298K} = 174.2 \text{ kJ/mol} \quad \text{(R1)}$$

The selected catalyst should promote the C–C bond rupture to produce CO_2, and/or CO and CH_4. The CO and CH_4 intermediates will be further converted to H_2 and CO_2. Coke formation should be avoided [6,7]. Current CSRE catalysts are mostly Ni- and Co-based [8], possibly with Ce-doping, and are discussed and evaluated below.

In the CSRE conversion, several competing reactions, as listed in Table 1, can however complement the main (R1) production route. Since operating at temperatures of 450 to 600 °C, it is unlikely that exothermic reactions will take place. Previous experimental results moreover demonstrated that acetone, acetaldehyde and carbon were not produced [8]. These secondary reactions can hence be excluded. The complex reaction paths of Table 1 were used in equilibrium calculations [9,10], and presented in Section 3.

CSRE will need to be operated at a low pressure since all the reactions see the number of product moles increased [1]. The equilibrium calculations of Section 3 below, and our experimental findings delineate the major reaction parameters of the ethanol conversion in terms of the molar ratio of steam/EtOH, operating temperature

and reaction time. To inhibit coke formation, the S/E ratio should exceed 2 and low temperatures (<450 °C) should be avoided [11,12].

Table 1. Competing reactions [9,10].

	ΔH^0 (kJ/mol)	Reference
$CH_3CH_2OH + 3H_2O \rightarrow 6H_2 + 2CO_2$	174.2	(R1)
$CH_3CH_2OH \rightarrow CH_3CHO + H_2$	68	(R2)
$CH_3CHO + H_2O \rightarrow 3H_2 + 2CO$	213	(R3)
$CH_3CH_2OH \rightarrow C_2H_4 + H_2O$	45	(R4)
$C_2H_4 \rightarrow$ Polymers $\rightarrow$ coke	Not available	(R5)
$2CH_3CH_2OH \rightarrow C_3H_6O + CO + 3H_2$	196	(R6)
$CH_3CH_2OH + H_2O \rightarrow 4H_2 + 2CO$	~225	(R7)
$CO + H_2O \rightarrow H_2 + CO_2$	−41	(R8)
$CH_3CH_2OH \rightarrow H_2 + CO + CH_4$	~50	(R9)
$2CO \rightarrow C + CO_2$	172	(R10)

The fermentative production of ethanol by first- and second-generation feedstock was assessed in detail by Kang et al. [3–5]. Whereas the first-generation processes are mature, the second-generation processes are continuously being developed and improved. Producing a 2nd generation bio-ethanol from corn stover is a sustainable and efficient example of utilizing agricultural waste and reduce dependence on fossil fuels [13]. Technical barriers involve the complex structure of the lignocellulosic biomass, which requires a pretreatment to degrade the lignin and extract the cellulose and hemicellulose [14–16]. Xylose in the enzymatic hydrolysate can moreover not be used by conventional microorganisms for bioethanol fermentation [17]. Additionally, the fermentation can be hindered by inhibitory compounds released during pretreatment, which can reduce the productivity of the microorganisms and decrease ethanol yields [18,19].

The unit processes in the whole production chain of the bio-ethanol production are described in Section 2.1 and Supplementary Information SI-2.

1.2. Reviewing Investigated Catalysts

The vapor-phase CSRE requires the application of efficient metal catalysts, referred to as active species, supported by a porous and stable carrier. Previous publications, as available from Web-of-Science data, and summarized by Deng et al. [8] were analyzed in order to classify all available data in terms of active species and supports, as illustrated in Supplementary Information, Tables S1 and S2, Figures S1–S4.

High activity, stability and avoiding coke formation are of essential importance [20]. The recent development mostly emphasizes the use of cheaper metal catalysts, such as Co, Ni and their bi-metallic combinations [21–25]. Catalyst coking and CH_4 formation are negligible [26].

Some specific catalyst-support combinations were not taken into consideration for the lack of complete data [27–31] and/or for the low H_2 yield, e.g., MnO, $MnFe_2O_4$, among others [26,29].

Co-based catalysts have been extensively investigated. The presence of both metallic Co^0 and Co^{2+} species is required to obtain a stable activity [32–41], while being accompanied by a negligible coking [42–44]. Whereas Co^0 sites foster C-C bond rupture, Co^{2+} sites increase the formation of water and acetate [45,46], that promptly react to CO, CO_2, and H_2 [46,47].

The Ni-catalyst species have also been studied. Both Co and Ni are applied onto similar supports with Al_2O_3 as the mostly used support [48–51]. Other supports were also proposed. Ni- and Co-based catalysts are active in breaking C-C bonds and for CH_4 steam conversion [26,52,53]. CSRE results when using the above-mentioned catalysts in a temperature range between 420 and 650 °C were presented by Deng et al. [8]. The promotion of the Co-activity by doping with Ce was proposed and further assessed in the present research.

Toward catalyst supports, zeolites, ceria and α-Al_2O_3 are mainly used. For CSRE, zeolites are however less recommendable due to the acid zeolite sites promoting ethanol dehydration instead of dehydrogenation [8]. Ceria was assessed by Hou et al. [54]. Thermally and chemically stable alumina (Al_2O_3) supports are commonly used in CSRE processes. α-Al_2O_3 is an appropriate support and its properties (e.g., porosity, BET) can be tailored to dehydrogenate EtOH. At a molar S/E ratio in excess of 2, the α-Al_2O_3 supported catalysts oppress carbon formation [6].

1.3. Objectives

The present research adds new findings to previous research results, and it will cover the following successive topics:

(i) manufacture and fully characterize the appropriate catalysts;
(ii) study the catalyst achievements at different CSRE conditions, using 2nd-generation bio-EtOH as feedstock;
(iii) investigate the H_2 production in function the S/E ratio, temperature and vapor residence time in the reactor;
(iv) determine the catalyst stability during long-duration (2000 h) testing;
(v) assess the kinetics of the CSRE reaction;
(vi) present results obtained in a the continuous solar (particle-driven) bio-EtOH conversion to H_2;
(vii) tentatively examine the present process economics of the present developments.

2. Experimental Methods and Procedures

2.1. Bio-Ethanol

Since outside the main scope of the present paper, the essentials of the production process and obtained results are given in Supplementary Information SI-2.

2.2. Experimental Set-Up for CSRE and Procedure

2.2.1. Preparing Metal or Multi-Metal Catalysts on α-Al_2O_3 Support

The investigated catalysts were produced by multiple iso-volumetric wet impregnation of the α-Al_2O_3 support using a (mixed) alcoholic solution of metal nitrate(s) to obtain a metal loading of about 10 wt%. Between successive impregnations, vacuum-drying at 90 °C for 1 h was applied. After completed impregnation, the catalysts were heat-treated for 5 h in air at 700 °C with a heat ramp of 10 °C/min. The metal cations were reduced during the initial CSRE hydrogen production.

The catalyst structure will be illustrated in Section 4.

2.2.2. Experimental Layouts

The experiments involved 2 different rigs. Initial selection and long-duration tests were performed in a vertical electrically-heated furnace. A pilot-scale particle-driven (solar) rig was tested, but full solar experiments will be re-started in the solar high season (from May 2025 onward). The rig was however operated also without the solar receiver, but by heating the particles before their circulation in a PV-power heated silo. Figure 1a,b illustrates the setup elements. A piston pump (LongerPump, Hebei) fed the EtOH/H_2O mixture to the CSRE reactor.

N_2 is used as carrier gas. All flows are measured. The feed flow is preheated before the catalytic bed section of the reactor. Product gas components were monitored by GC-MS after cooling and dehumidification. Figure 1b illustrates the pilot setup. The bed depths were 15 cm in the electrically-heated reactors, while 25 cm in the pilot reactor.

The solar-PV set-up was partly used in the laboratory, where PV-electricity was converted into particle sensible heat, and applied afterwards as illustrated in Figure 1b. The applied analytical techniques are summarized in Table 2.

For Figure 1b,c the units comprise the following unit processes:

1. Cavity and receiver
2. Storage of inert particle carrier, with electrical heating (PV)
3. Screw conveyor(s)
4. Moving-bed indirect CSRE reactor (Multi-tubular CSRE reactor with indirect heating by particle loop)
5. Conveying of carrier-particles to 1

Experimental results were transformed into conversion yield and selectivity following:

Conversion (%) = $\frac{n_{EtOH}^{in} - n_{EtOH}^{out}}{n_{EtOH}^{in}} \times 100$

H_2 yield (%) = $\frac{n_{H_2}^{out}}{6 \times n_{EtOH}^{in}} \times 100$, with 6 is the molar ratio of H_2 and EtOH in (R1).

H_2 selectivity (%) = $\frac{n_{H_2}^{out}}{n_{H_2}^{out} + 2n_{CH_4}^{out}} \times 100$

Results will also be transformed into reaction kinetics and will include catalyst properties when expressed as hourly space velocities, SY:

$$\text{SY} = \frac{\text{flow rate of } H_2 \text{ in Nm}^3 \text{ or mol/h}}{\text{weight of catalyst}} = \frac{\text{Nm}^3 \text{ or mol}}{h\ g_{cat}}$$

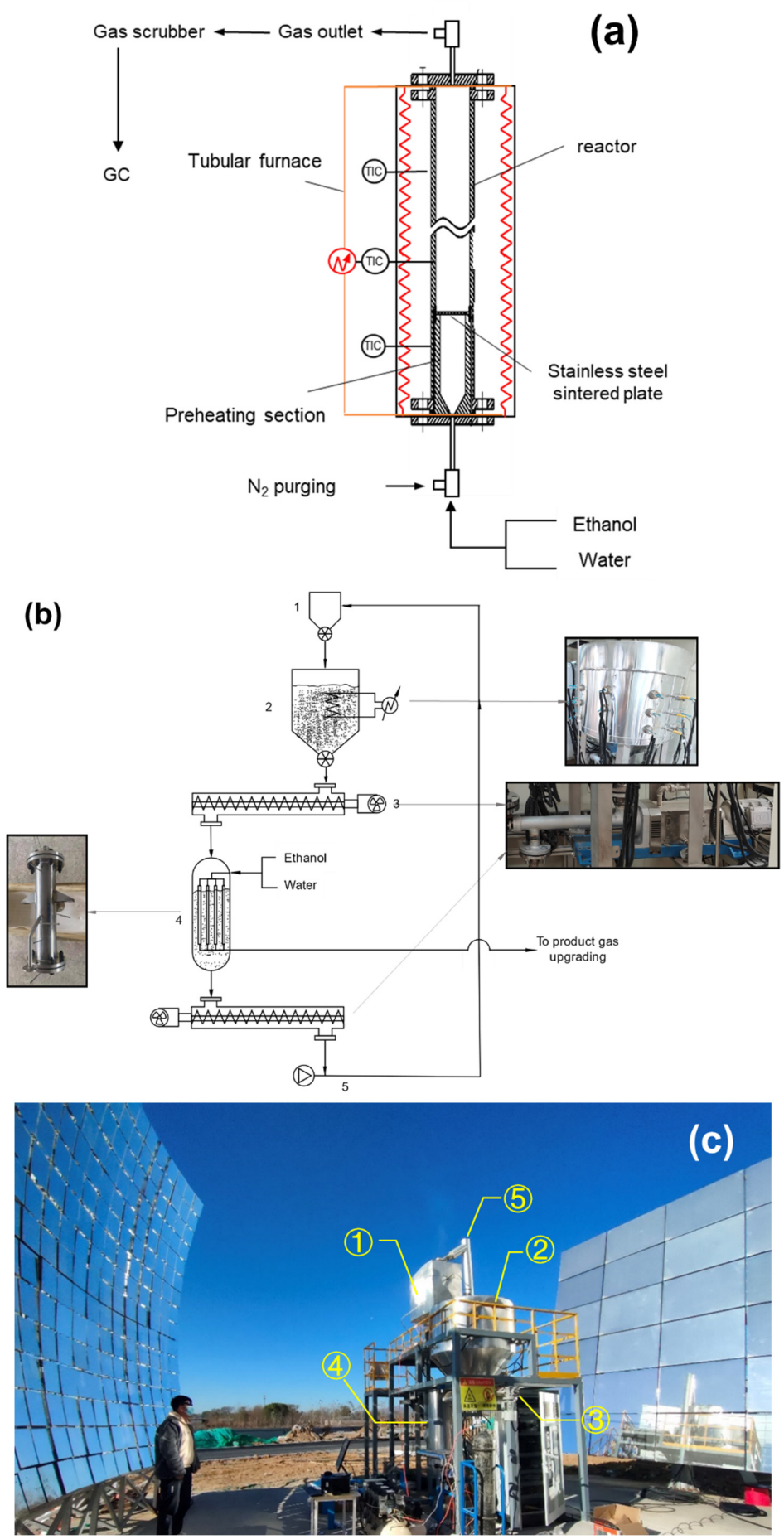

Figure 1. (**a**). Tubular furnace experimental set-up [ZSHIEZD Inc., USA], (**b**). Layout of the pilot particle driven (solar) CSRE process [BUCT, CN], (**c**). Overall illustration of solar concentrator, heat storage and reactor.

Table 2. Different analytical techniques.

Measurement	Parameter	Analyzer
Co and Ce-content in the catalyst	Co, Ni in wt%	ICP-OES 5800 Agilent spectrometer
Specific surface area, as BET	Total surface area in m^2/g	Quantachrome Nova 4000e Micromeritics
H_2, CO, CO_2, CH_4 and $C_xH_yO_z$ concentrations	All concentration in vol% of product gas	BFRL Thermal conductivity meter (TCD)
Carbon product morphology by scanning electron microscope (SEM)	Particle size in nm or μm	TESCAN MIRA LMS
Temperature, pressure and flow rates	T (°C), p (Pa), Q (mL/min)	Standard T and P probes, and mass flow meters

3. Reaction Equilibrium

The thermo-catalytic CSRE is characterized by its reaction kinetics and its thermodynamic equilibria. The equilibria of the complex and combined reactions (R1) to (R10) were studied between 450 °C and 650 °C. Reactions of Figure 2 with a positive Gibbs' free energy, ΔG^0, at the expected range of operating temperatures were not considered.

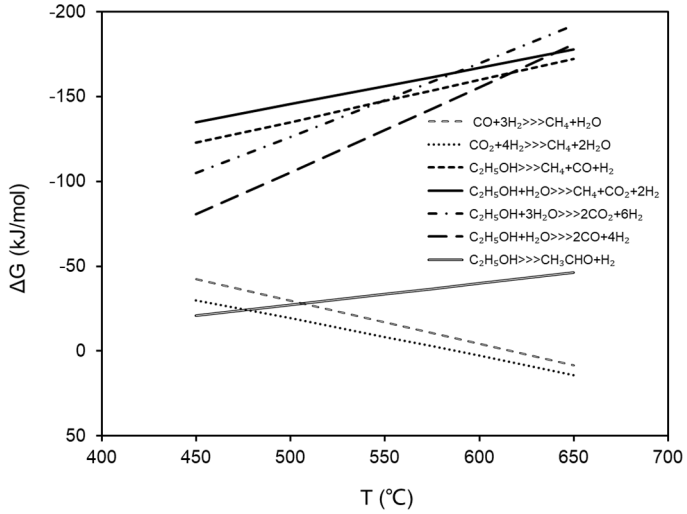

Figure 2. ΔG versus temperature for the possible reactions.

Aspen Plus (version 11) "REQUIL" and "RGIBBS" software were used to examine the effects of different T and S/E operating modes, as presented in Figure 3 [55,56].

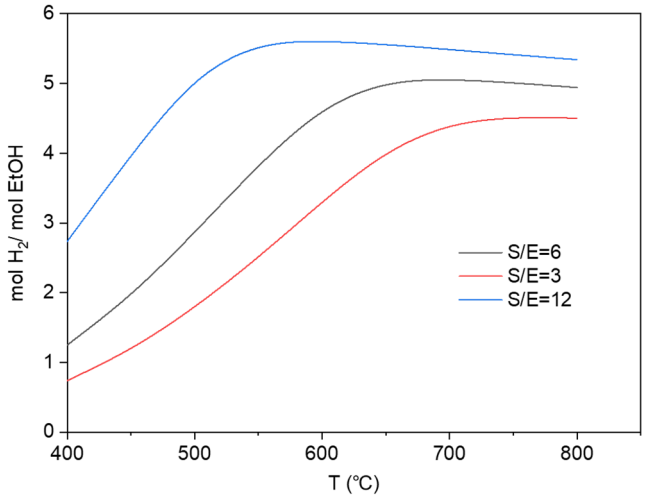

Figure 3. Equilibrium H_2 concentration versus temperature for specified S/E molar ratios.

The S/E ratio is important, and values above 12 are recommended for temperatures in excess of about 480 °C.

4. Detailed Results and Discussion

4.1. H_2 Production by CSRE

4.1.1. Preliminary Screening of Previous and Own Catalysts

Some single or compound catalysts were assessed during >30 h of CSRE. These results were in line with literature data and reported by Deng et al. [8].

10Co/α-Al_2O_3 (10wt% Co) provided excellent results. Multi-metal catalyst, especially with Ce doping, slightly increased the H_2 yield of mono-metal catalysts. Further experiments hence concentrated on the Co-supported and Co-CeO_2 catalysts.

4.1.2. Results for the Co/α-Al_2O_3 and Co-CeO_2/α-Al_2O_3 Catalyst System

The results are provided in Table 3 below. 10Co refers to a Co-loading of 10 wt%.

Table 3. Lab-scale experimental results at specified conditions.

10Co/α-Al_2O_3 System at Different Reaction Temperatures (S/E = 6)					
T	**mol X/mol EtOH**				**H_2 yield (%)**
	H_2	**CO**	**CH_4**	**CO_2**	
450 °C	3.882	0.136	0.247	1.003	64.7
500 °C	4.605	0.290	0.143	1.112	76.8
550 °C	5.074	0.430	0.056	1.258	84.6
600 °C	5.430	0.624	0.026	1.248	90.5
10Co/α-Al_2O_3 system at different S/E (at 450 °C, same EtOH feed rate)					
S/E = 3	3.421	0.293	0.430	0.759	57.0
S/E = 4	3.522	0.242	0.260	0.837	58.7
S/E = 6	3.882	0.137	0.247	1.003	64.7
S/E = 10	4.711	0.206	0.227	1.412	78.5
S/E = 20	5.074	0.097	0.170	1.674	84.6
5Co-5CeO_2/α-Al_2O_3 system at different reaction temperatures and S/E = 6					
450 °C	4.202	0.042	0.378	1.223	70.0
500 °C	4.550	0.105	0.390	1.363	75.8
550 °C	4.818	0.124	0.266	1.437	80.3
600 °C	5.302	0.206	0.208	1.541	88.4
5Co-5CeO_2/α-Al_2O_3 system at different S/E (at 450 °C, same EtOH feed rate)					
S/E = 3	3.314	0.015	0.476	1.029	55.2
S/E = 4	3.895	0.026	0.314	1.181	64.9
S/E = 6	4.202	0.042	0.378	1.223	70.0
S/E = 10	4.751	0.026	0.172	1.413	79.2
S/E = 20	5.229	0.045	0.120	1.596	87.1
8Co-2CeO_2/α-Al_2O_3 system at different reaction temperatures and S/E = 6					
450 °C	4.045	0.043	0.381	1.137	67.4
500 °C	4.870	0.093	0.260	1.422	81.2
550 °C	5.346	0.045	0.164	1.689	89.1
600 °C	5.781	0.001	0.169	1.881	96.3
8Co-2CeO_2/α-Al_2O_3 system at different contact time (at 500 °C)					
7.231 s	5.839	0.129	0.131	1.958	97.3
3.616 s	5.523	0.115	0.139	1.875	92.1
2.410 s	5.247	0.109	0.159	1.771	87.5
1.808 s	5.219	0.128	0.164	1.828	87.0
1.205 s	5.159	0.117	0.158	1.783	86.0
8Co-2CeO_2/α-Al_2O_3 system at different S/E (at 500 °C, same EtOH feed rate)					
S/E = 3	4.374	0.482	0.443	0.907	72.9
S/E = 4	4.724	0.446	0.315	1.158	78.7
S/E = 6	4.870	0.093	0.260	1.422	81.2
S/E = 10	5.605	0.090	0.160	1.689	93.4
S/E = 20	5.669	0.062	0.139	1.751	94.5

It is clear that the 8Co-2CeO_2/α-Al_2O_3 operates at the highest H_2-yield for a selected optimum T (550~600 °C) and a long contact time. Long-duration results (2000 h) are illustrated in Figure 4, for the selected 8Co-2CeO_2/α-

Al_2O_3 catalyst at S/E = 12 and 500 °C. The product composition is stable and almost constant. Negligible CH_4 concentrations are detected and hence confirm the equilibrium calculations.

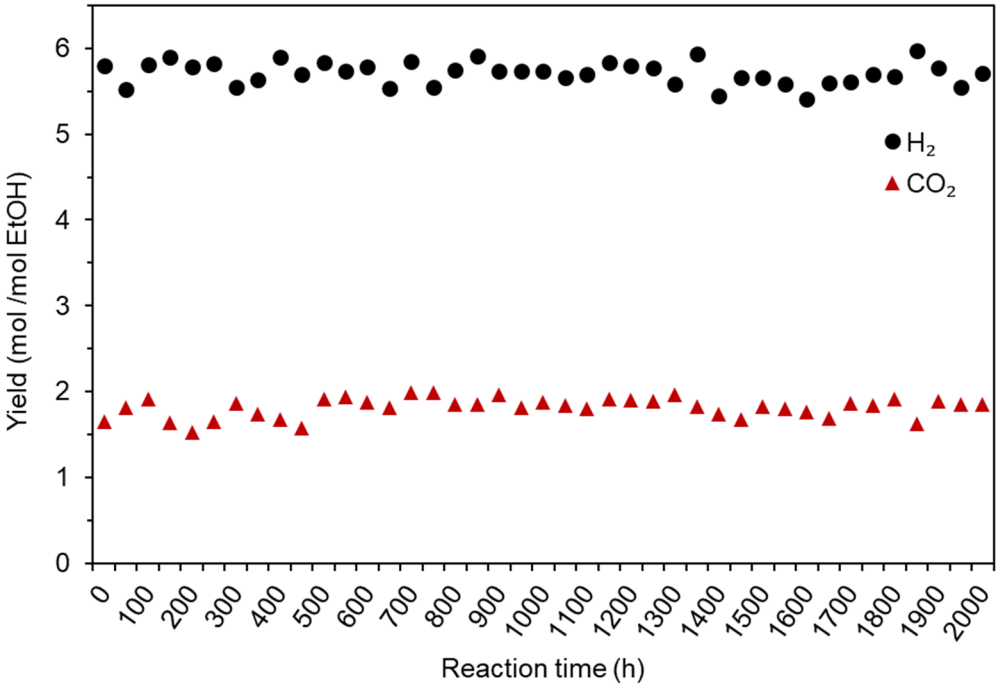

Figure 4. Stable H_2 production yield for continuous 2000 h operation with 17.2 wt% EtOH feed. mol/mol EtOH composition: H_2: 5.71 ± 0.26; CO_2: 1.819 ± 0.29 (CO and CH_4 concentrations were below 0.2 mol /mol EtOH and are not presented in the Figure: CO: 0.09 ± 0.03; CH_4: 0.15 ± 0.02).

SEM analyses demonstrate the stability of the 8Co-2CeO_2/α-Al_2O_3 catalyst, as illustrated in Figure 5. The 8Co-2CeO_2/α-Al_2O_3 catalyst is highly performing, without coking and with very low CH_4 produced. The 600 °C conversion on different catalysts was nearly complete, with minor changes in product distribution over time, as dealt with in the section below. Similar plots can be obtained for all experimental results of Table 3.

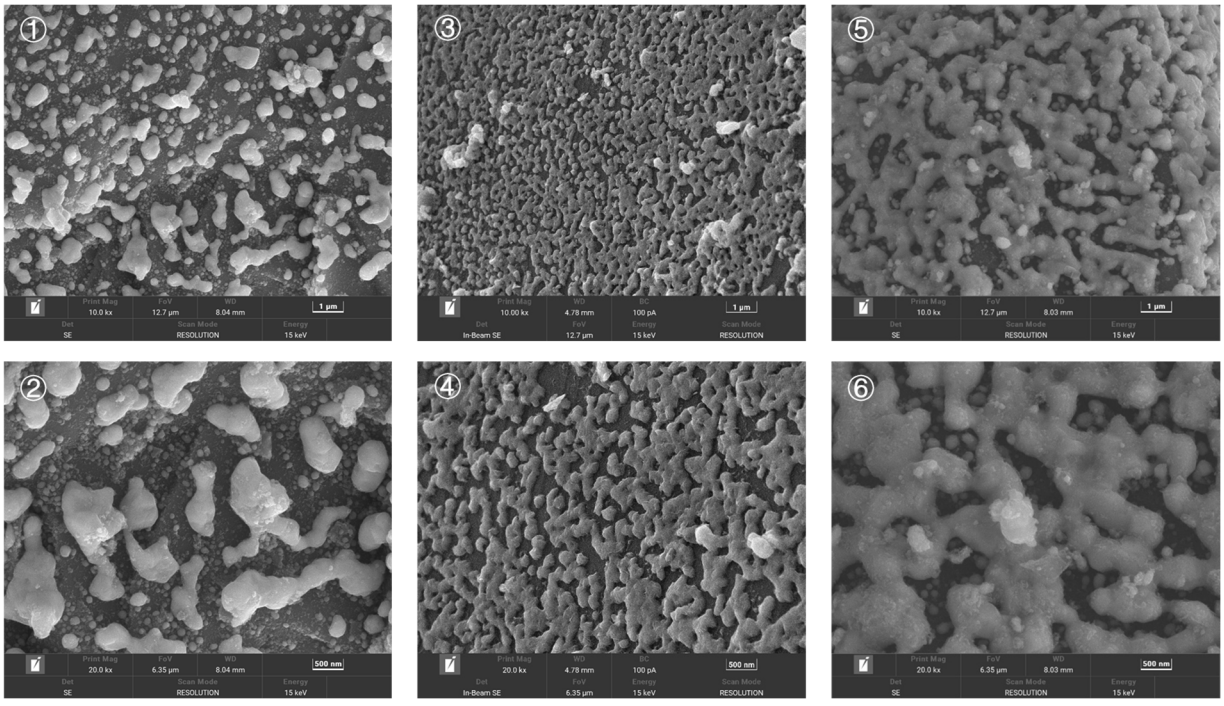

Figure 5. Experimental results of SEM of 8Co-2CeO_2/α-Al_2O_3 catalyst system before the H_2 process, after the H_2 process and after 2000 h of reaction (at 17.2 wt% EtOH concentration). (①,② before the H_2 process, ③,④ after the H_2 process, ⑤,⑥ after 2000 h of reaction).

4.3. Kinetics

The reaction kinetics can be determined from the experimental conversion versus time.

A 4th order Runge Kutta treatment was applied to solve the combined differential equations [57–59]. It was assumed that the EtOH conversion to CO_2 and CO is of 1st order and irreversible. Due to the high S/E ratio, the H_2O concentration can be assumed as constant [8,60] and hence not included in the reaction rate equation. CH_4 formation is formed to a negligible. Experimental and predicted product concentrations versus reaction time are given in Figure 6, and confirm a very good agreement.

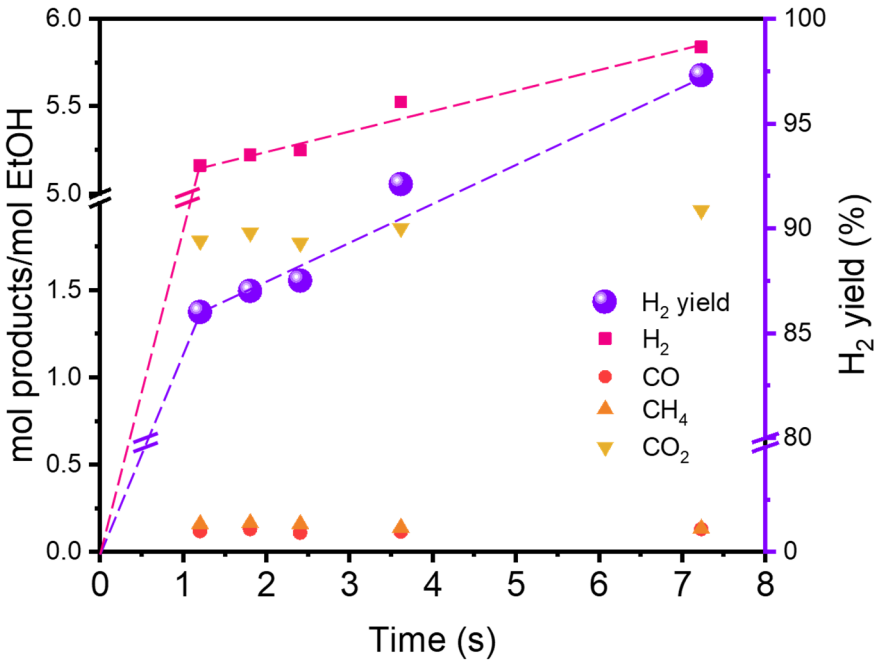

Figure 6. Experimental and predicted reaction kinetics for 8Co-2CeO_2/α-Al_2O_3 CSRE at 500 °C.

The 5.8 mol H_2/mol EtOH yield corresponds with the previous equilibrium concentrations and is reached for contact times exceeding 3 to 4 s, where also ~1.8 mol CO_2/mol EtOH is measured. The CH_4 and CO concentrations are low at all contact times. The CSRE conversion of EtOH follows a fast reaction rate. Equilibrium is already achieved at 7 s. In using a first order reaction rate expression, the experimental rate constant k is ~ 0.43 s^{-1}.

The predictions reveal the kinetic constants k_1 (H_2) and k_2(CO_2), as 0.293 and 0.112 s^{-1}, respectively. The sum of both k-values is close to the overall rate conversion, k.

With an active species weight of 45 g, the hourly space velocity (SY) is obtained.

For 8Co-2CeO_2/α-Al_2O_3 catalyst, SY-values of 7.0 L H_2 g_{cat}^{-1} h^{-1} or 0.31 mol H_2 g_{cat}^{-1} h^{-1} at 500 °C, and 8 L H_2 g_{cat}^{-1} h^{-1} or 0.35 mol H_2 g_{cat}^{-1} h^{-1} at 600 °C are obtained.

5. Pilot-Scale Research Developments

5.1. Solar Particle-Driven CSRE

Future applications of the CSRE concept in a low-carbon scenario should indeed use curtailed PV, wind or concentrated solar energy. In the concentrated solar reactor, heliostats focus the solar radiation on a cavity receiver. Geometrical and operating parameters were given in Deng et al. [8], and involve a reaction T of 600 °C.

Due to the intermittent solar irradiation at the test site, the daily testing duration was limited to 4–4.5 h at an average DNI of ~0.5 kW/m^2.

In off-sun periods, the electrical particle heating and successive CSRE loop of Figure 2b was used in repeat runs, each during 1 week. To avoid operating at high temperatures that are only achievable in the concentrated solar reactor, the CSRE-temperatures were limited to 480 ± 20 °C. Despite these low temperatures, a hydrogen yield of about 5 mol H_2/mol EtOH was achieved. The electrical heating of the particles in the loop is currently increased to 600 °C. The feed rate of the 17.2 wt% EtOH-water mixture was 0.2 mL/min. Results are given in Table 4 and Figure 7. These results are close to the yields previously obtained in fixed beds as reported in Section 4. Testing in the concentrated solar loop will be re-started in May 2025 (periods of high DNI).

Table 4. Average solar-PV results (8 days of 4 h at DNI of 0.5 kW/m^2 and 480 ± 20 °C).

Temperature (°C)	Catalyst	H_2 yield (%)	mol H_2/ mol EtOH	C selectivity (mol/mol Ethanol)		
				CO_2	CO	CH_4
480 ± 20 °C	8Co-2CeO_2/α-Al_2O_3	83.3	5.00	1.72	0.04	0.24
600 ± 20 °C	8Co-2CeO_2/α-Al_2O_3	95.3	5.72	1.84	0.03	0.13

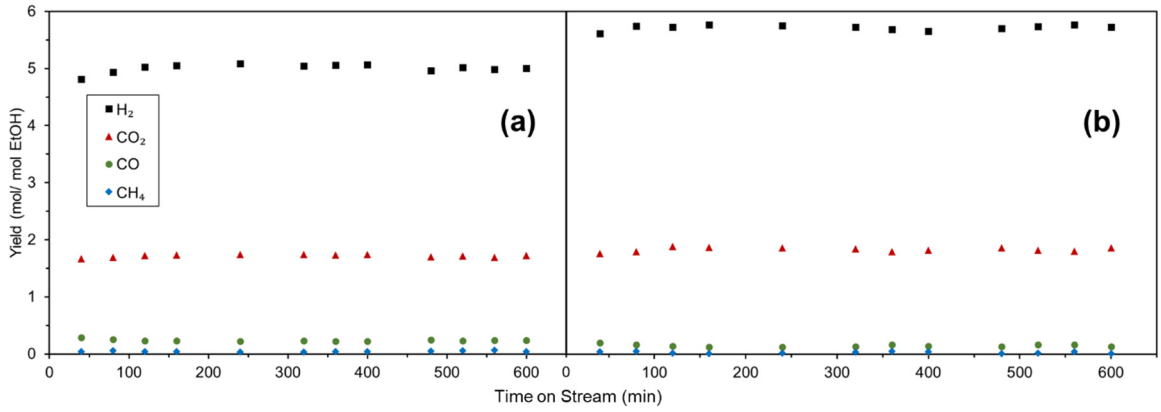

Figure 7. CSRE decomposition results in the solar-PV experiments, (**a**) at 480 ± 20 °C, (**b**) at 600 ± 20 °C.

The results demonstrate that lower temperatures produce slightly lower CO_2 product concentrations than in the long-duration experiments (see Figure 5), hence implying higher CO and CH_4 concentrations to close the C-balance.

5.2. Preliminary Process Economics

Despite having operated the pilot-scale CSRE in a concentrated solar and PV-driven operation mode, and having demonstrated that a long-duration stable operation of the CSRE principle is possible, the process is still considered at Technology Readiness Level (TRL) of 1 to 3. It is yet too early to present relevant values of the required plant investments.

We can however estimate the production cost of H_2 from the experimental results and the process data.

Second-generation bio-ethanol, produced from an agro-waste i.e., corn stover, offers a cost benefit versus first generation carbohydrate bio-EtOH. The corn stover process moreover offers the possibility of a flash evaporation after the fermentation to yield clean EtOH-water mixtures of the desirable concentration.

The cost of the stover-based bio-EtOH will be ~400 $/ton EtOH (against at least 700 $/ton for the 1st generation alternative) [61,62].

Since the CSRE will produce over 5.6 mol H_2/mol EtOH, 1 kg of EtOH will yield 0.217 kg H_2.

The experimental rig operated at 0.2 mL/min with 82.8 wt% H_2O and 17.2 wt% EtOH.

The supplied heat load, including insulation heat losses, was 14 W to include 9.35 W for H_2O heating and evaporation, 1.15 W for EtOH heating and evaporation, and 2.17 W for the reaction heat.

With a heat recovery on the product gas, ~4 W could be recovered and re-used as process heat.

The remaining 10 W were either supplied by concentrated solar irradiance or by PV.

Extrapolating these findings to a 50 kg/h (13.9 g/s) feed at 17.2 wt% EtOH, the total required heat will be 58.3 kW. With a good heat recovery, 18.3 kW could be recovered. The external heat duty will hence be above 40 kW.

This can easily be supplied by PV-electricity or concentrated solar heat. If we would burn the corn stover residue to supply the heat requirements, we would need to feed 9.6 kg/h of residue to the combustor. Assuming a power cost of 0.1 $/kW, the raw material cost (400 $/ton) will determine the production value of H_2.

The H_2 production will be 10.88 kg/h and the H_2 product value will be around 2 $/kg H_2. Of course this net cost must be increased by other direct and indirect operation costs, and a preliminary estimate confirms a price of between 3 and 3.5 $/kg H_2, far below the price of electrolysis H_2.

6. Conclusions

The present research combined the second-generation fermentation of an agro-industrial residue, i.e., corn stover, with the catalytic steam reforming of the produced bio-ethanol.

After fermentation, a bio-ethanol of appropriate H_2O content was obtained by flash concentration. In most of the experiments, a concentration of ~ 12 mol H_2O/mol EtOH was applied. Lower steam/ethanol (S/E) ratios were also tested to assess the S/E effect.

To prove the stability of the selected 8Co-2CeO_2/α-Al_2O_3 catalyst, experiments were continuously performed during 2000 h. Ethanol was over 95% converted. The carbon balance was closed by the CO_2 formed (only minor concentrations of CO and CH_4 were detected).

Initial tests in a (solar-PV and concentrated solar) particle-driven pilot rig confirmed the CSRE results but additional testing continues.

Kinetics of the CSRE are moderately fast (k = 0.43 s^{-1}). The catalyst utilization rate is 0.35 mol H_2 g_{cat}^{-1} h^{-1} at 600 °C.

Finally a production cost of H_2 was estimated when using renewable energy and bio-ethanol. H_2 production costs are predicted as 3.0 to 3.5 $/kg, much cheaper than electrolytic H_2. These results demonstrate that further solar CSRE research is justified.

Supplementary Materials: The following supporting information can be downloaded at: https://media.sciltp.com/articles/others/2509081508102572/SEE-0277-for-publish-SI.pdf. References [63–105] are cited in Supplementary Materials.

Author Contributions: Validation, Z.L. and S.L.; Investigation, Z.L. and Y.W.; Resources, M.Y. and S.L.; Formal Analysis, Y.W.; Writing—Original Draft, H.Z. and J.B.; Writing—Review & Editing, all authors; Visualization, Z.L., M.Y., S.L. and H.Z.; Supervision, H.Z. All authors have read and agreed to the published version of the manuscript.

Funding: The research was supported by the Beijing Advanced Innovation Center for Soft Matter Science and Engineering of Beijing University of Chemical Technology. Authors acknowledge the research funding from the National Key R&D Program of China [grant number 2021YFC2103705].

Data Availability Statement: Additional information requests can be directed to and will be fulfilled by the Lead Contact, Tianwei Tan (twtan@mail.buct.edu.cn) and/or by Huili Zhang (zhhl@mail.buct.edu.cn).

Conflicts of Interest: The authors declare no conflicts of interest.

Abbreviations

C_{eq}, C_t	Concentration at equilibrium and at time t, respectively	mol/Nm^3
k	Rate constant of the 1st order reaction	s^{-1}
t	Time	s
T	Operating temperature	°C
ΔH^0	Heat of reaction	kJ/mol
ΔH	Total heat load	kJ/h
DNI	Direct normal irradiance	kW/m^2
CSRE	Catalytic Stream Reforming of Ethanol	
PV	Photovoltaic Electricity	

References

1. Deng, Y.; Li, S.; Appels, L.; Dewil, R.; Zhang, H.; Baeyens, J.; Mikulčić, H. Producing hydrogen by catalytic steam reforming of methanol using non-noble metal catalysts. *J. Environ. Manag.* **2022**, *321*, 116019. https://doi.org/10.1016/j.jenvman.2022.116019.
2. Li, Z.; Zhang, H.; Dewil, R.; Deng, Y.; Li, S. Co-Al and Mn-Fe Catalytic Steam Reforming of CH_3OH to H_2. *IOP Conf. Ser. Earth Environ. Sci.* **2022**, *952*, 012007. https://doi.org/10.1088/1755-1315/952/1/012007.
3. Kang, Q.; Appels, L.; Tan, T.; Dewil, R. Bioethanol from Lignocellulosic Biomass: Current Findings Determine Research Priorities. *Sci. World J.* **2014**, *2014*, 298153. https://doi.org/10.1155/2014/298153.
4. Baeyens, J.; Kang, Q.; Appels, L.; Dewil, R.; Lv, Y.; Tan, T. Challenges and opportunities in improving the production of bio-ethanol. *Prog. Energy Combust. Sci.* **2015**, *47*, 60–88. https://doi.org/10.1016/j.pecs.2014.10.003.
5. Kang, Q.; Tan, T. Exergy and CO_2 Analyses as Key Tools for the Evaluation of Bio-Ethanol Production. *Sustainability* **2016**, *8*, 76. https://doi.org/10.3390/su8010076.
6. Sun, Z.; Shi, W.; Smith, L.R.; Dummer, N.F.; Qi, H.; Sun, Z.; Hutchings, G.J. Concerted catalysis of single atom and nanocluster enhances bio-ethanol activation and dehydrogenation. *Nat. Commun.* **2025**, *16*, 3935. https://doi.org/10.1038/s41467-025-59127-0.
7. Pyatnitsky, Y.; Dolgykh, L.; Stolyarchuk, I.; Strizhak, P. Analysis of the hydrogen yield for the ethanol steam reforming. *Biomass Convers. Biorefinery* **2024**, *14*, 23143–23150. https://doi.org/10.1007/s13399-023-04544-8.
8. Deng, Y.; Li, S.; Appels, L.; Zhang, H.; Sweygers, N.; Baeyens, J.; Dewil, R. Steam reforming of ethanol by non-noble metal catalysts. *Renew. Sustain. Energy Rev.* **2023**, *175*, 113184. https://doi.org/10.1016/j.rser.2023.113184.
9. Ni, M.; Leung, D.Y.C.; Leung, M.K.H. A review on reforming bio-ethanol for hydrogen production. *Int. J. Hydrogen*

Energy **2007**, *32*, 3238–3247. https://doi.org/10.1016/j.ijhydene.2007.04.038.

10. Palanisamy, A.; Soundarrajan, N.; Ramasamy, G. Analysis on production of bioethanol for hydrogen generation. *Environ. Sci. Pollut. Res.* **2021**, *28*, 63690–63705. https://doi.org/10.1007/s11356-021-14554-6.
11. Schwab, G.M. Cinétique Chimique Appliquée. *Z. Für Phys. Chem.* **1960**, *24*, 283–284. https://doi.org/10.1524/zpch.1960.24.3_4.283.
12. Liu, Q.; Zhou, H.; Jia, Z. Hydrogen Production by Ethanol Reforming on Supported Ni-Cu Catalysts. *ACS Omega* **2022**, *7*, 4577–4584. https://doi.org/10.1021/acsomega.1c06579.
13. Wu, Y.; Wei, J.; Wang, K.; Su, C.; Chen, C.; Cui, Z.; Cai, D.; Cheng, S.; Cao, H.; Qin, P. Understanding the Dynamics of the Saccharomyces cerevisiae and Scheffersomyces stipitis Abundance in Co-culturing Process for Bioethanol Production from Corn Stover. *Waste Biomass Valorization* **2023**, *14*, 43–55. https://doi.org/10.1007/s12649-022-01861-3.
14. Li, P.; Cai, D.; Luo, Z.; Qin, P.; Chen, C.; Wang, Y.; Zhang, C.; Wang, Z.; Tan, T. Effect of acid pretreatment on different parts of corn stalk for second generation ethanol production. *Bioresour. Technol.* **2016**, *206*, 86–92. https://doi.org/10.1016/j.biortech.2016.01.077.
15. Li, P.; Cai, D.; Zhang, C.; Li, S.; Qin, P.; Chen, C.; Wang, Y.; Wang, Z. Comparison of two-stage acid-alkali and alkali-acid pretreatments on enzymatic saccharification ability of the sweet sorghum fiber and their physicochemical characterizations. *Bioresour. Technol.* **2016**, *221*, 636–644. https://doi.org/10.1016/j.biortech.2016.09.075.
16. Wu, Y.; Wen, J.; Su, C.; Jiang, C.; Zhang, C.; Wang, Y.; Jiang, Y.; Ren, W.; Qin, P.; Cai, D. Inhibitions of microbial fermentation by residual reductive lignin oil: Concerns on the bioconversion of reductive catalytic fractionated carbohydrate pulp. *Chem. Eng. J.* **2023**, *452*, 139267. https://doi.org/10.1016/j.cej.2022.139267.
17. Li, Y.J.; Wang, M.M.; Chen, Y.W.; Wang, M.; Fan, L.H.; Tan, T.W. Engineered yeast with a CO_2-fixation pathway to improve the bio-ethanol production from xylose-mixed sugars. *Sci. Rep.* **2017**, *7*, 43875. https://doi.org/10.1038/srep43875.
18. Brandt, B.A.; Jansen, T.; Görgens, J.F.; van Zyl, W.H. Overcoming lignocellulose-derived microbial inhibitors: Advancing the Saccharomyces cerevisiae resistance toolbox. *Biofuels Bioprod. Biorefining* **2019**, *13*, 1520–1536. https://doi.org/10.1002/bbb.2042.
19. Qin, L.; Dong, S.; Yu, J.; Ning, X.; Xu, K.; Zhang, S.J.; Xu, L.; Li, B.Z.; Li, J.; Yuan, Y.J.; et al. Stress-driven dynamic regulation of multiple tolerance genes improves robustness and productive capacity of Saccharomyces cerevisiae in industrial lignocellulose fermentation. *Metab. Eng.* **2020**, *61*, 160–170. https://doi.org/10.1016/j.ymben.2020.06.003.
20. Ogo, S.; Sekine, Y. Recent progress in ethanol steam reforming using non-noble transition metal catalysts: A review. *Fuel Process. Technol.* **2020**, *199*, 106238. https://doi.org/10.1016/j.fuproc.2019.106238.
21. Vaidya, P.D.; Rodrigues, A.E. Insight into steam reforming of ethanol to produce hydrogen for fuel cells. *Chem. Eng. J.* **2006**, *117*, 39–49. https://doi.org/10.1016/j.cej.2005.12.008.
22. Bion, N.; Duprez, D.; Epron, F. Design of Nanocatalysts for Green Hydrogen Production from Bioethanol. *ChemSusChem* **2012**, *5*, 76–84. https://doi.org/10.1002/cssc.201100400.
23. Homsi, D.; Rached, J.A.; Aouad, S.; Gennequin, C.; Dahdah, E.; Estephane, J.; Tidahy, H.L.; Aboukaïs, A.; Abi-Aad, E. Steam reforming of ethanol for hydrogen production over Cu/Co-Mg-Al-based catalysts prepared by hydrotalcite route. *Environ. Sci. Pollut. Res.* **2017**, *24*, 9907–9913. https://doi.org/10.1007/s11356-016-7480-9.
24. Souza, J.P.; Freitas, P.E.; Almeida, L.D.; Rosmaninho, M.G. Development of new materials from waste electrical and electronic equipment: Characterization and catalytic application. *Waste Manag.* **2017**, *65*, 104–112. https://doi.org/10.1016/j.wasman.2017.03.051.
25. Strizhak, P.E.; Pyatnitsky, Y.I.; Dolgikh, L.Y.; Kosmambetova, G.R.; Trypolskyi, A.I.; Kalishyn, Y.Y., Bychko, I.B. Nanosize Effect in Heterogeneous Catalytic Processes Over Copper, Iron, and Zirconium Oxides. *Theor. Exp. Chem.* **2017**, *53*, 305–314. https://doi.org/10.1007/s11237-017-9530-x.
26. Sharma, Y.C.; Kumar, A.; Prasad, R.; Upadhyay, S.N. Ethanol steam reforming for hydrogen production: Latest and effective catalyst modification strategies to minimize carbonaceous deactivation. *Renew. Sustain. Energy Rev.* **2017**, *74*, 89–103. https://doi.org/10.1016/j.rser.2017.02.049.
27. Gonçalves, A.A.S.; Faustino, P.B.; Assaf, J.M.; Jaroniec, M. One-Pot Synthesis of Mesoporous Ni-Ti-Al Ternary Oxides: Highly Active and Selective Catalysts for Steam Reforming of Ethanol. *ACS Appl. Mater. Interfaces* **2017**, *9*, 6079–6092. https://doi.org/10.1021/acsami.6b15507.
28. Sharma, S.; Patil, B.; Pathak, A.; Ghosalkhar, S.; Mohanta, H.K.; Roy, B. Application of BICOVOX catalyst for hydrogen production from ethanol. *Clean Technol. Environ. Policy* **2018**, *20*, 695–701. https://doi.org/10.1007/s10098-017-1394-1.
29. Campos, C.H.; Pecchi, G.; Fierro, J.L.G.; Osorio-Vargas, P. Enhanced bimetallic Rh-Ni supported catalysts on alumina doped with mixed lanthanum-cerium oxides for ethanol steam reforming. *Mol. Catal.* **2019**, *469*, 87–97. https://doi.org/10.1016/j.mcat.2019.03.007.
30. Nejat, T.; Jalalinezhad, P.; Hormozi, F.; Bahrami, Z. Hydrogen production from steam reforming of ethanol over Ni-Co bimetallic catalysts and MCM-41 as support. *J. Taiwan Inst. Chem. Eng.* **2019**, *97*, 216–226. https://doi.org/10.1016/j.jtice.2019.01.025.

31. Rodrigues, T.S.; de Moura, A.B.L.; e Silva, F.A.; Candido, E.G.; da Silva, A.G.M.; de Oliveira, D.C.; Quiroz, J.; Camargo, P.H.C.; Bergamaschi, V.S.; Ferreira, J.C.; et al. Ni supported $Ce_{0.9}Sm_{0.1}O_{2-\delta}$ nanowires: An efficient catalyst for ethanol steam reforming for hydrogen production. *Fuel* **2019**, *237*, 1244–1253. https://doi.org/10.1016/j.fuel.2018.10.053.
32. Ogo, S.; Maeda, S.; Sekine, Y. Coke Resistance of Sr-Hydroxyapatite Supported Co Catalyst for Ethanol Steam Reforming. *Chem. Lett.* **2017**, *46*, 729–732. https://doi.org/10.1246/cl.170072.
33. de Lima, A.E.P.; de Oliveira, D.C. In situ XANES study of Cobalt in Co-Ce-Al catalyst applied to Steam Reforming of Ethanol reaction. *Catal. Today* **2017**, *283*, 104–109. https://doi.org/10.1016/j.cattod.2016.02.029.
34. Sohn, H.; Soykal, I.I.; Zhang, S.; Shan, J.; Tao, F.; Miller, J.T.; Ozkan, U.S. Effect of Cobalt on Reduction Characteristics of Ceria under Ethanol Steam Reforming Conditions: AP-XPS and XANES Studies. *J. Phys. Chem. C* **2016**, *120*, 14631–14642. https://doi.org/10.1021/acs.jpcc.6b02490.
35. Chen, M.;Wang, C.; Wang, Y.; Tang, Z.; Yang, Z.; Zhang, H.; Wang, J. Hydrogen production from ethanol steam reforming: Effect of Ce content on catalytic performance of Co/Sepiolite catalyst. *Fuel* **2019**, *247*, 344–355. https://doi.org/10.1016/j.fuel.2019.03.059.
36. Kim, K.M.; Kwak, B.S.; Im, Y.; Park, N.K.; Lee, T.J.; Lee, S.T.; Kang, M. Effective hydrogen production from ethanol steam reforming using CoMg co-doped SiO_2@$Co_{1-x}Mg_xO$ catalyst. *J. Ind. Eng. Chem.* **2017**, *51*, 140–152. https://doi.org/10.1016/j.jiec.2017.02.025.
37. Sohn, H.; Celik, G.; Gunduz, S.; Dogu, D.; Zhang, S.; Shan, J.; Tao, F.F.; Ozkan, U.S. Oxygen Mobility in Pre-Reduced Nano- and Macro-Ceria with Co Loading: An AP-XPS, In-Situ DRIFTS and TPR Study. *Catal. Lett.* **2017**, *147*, 2863–2876. https://doi.org/10.1007/s10562-017-2176-4.
38. Ogo, S.; Shimizu, T.; Nakazawa, Y.; Mukawa, K.; Mukai, D.; Sekine, Y. Steam reforming of ethanol over K promoted Co catalyst. *Appl. Catal. A Gen.* **2015**, *495*, 30–38. https://doi.org/10.1016/j.apcata.2015.01.018.
39. Passos, A.R.; Martins, L.; Pulcinelli, S.H.; Santilli, C.V.; Briois, V. Correlation of Sol-Gel Alumina-Supported Cobalt Catalyst Processing to Cobalt Speciation, Ethanol Steam Reforming Activity, and Stability. *ChemCatChem* **2017**, *9*, 3918–3929. https://doi.org/10.1002/cctc.201700319.
40. Turczyniak, S.; Greluk, M.; Slowik, G.; Gac, W.; Zafeiratos, S.; Machocki, A. Surface State and Catalytic Performance of Ceria-Supported Cobalt Catalysts in the Steam Reforming of Ethanol. *ChemCatChem* **2017**, *9*, 782–797. https://doi.org/10.1002/cctc.201601343.
41. Passos, A.R.; Fontaine, C.L.; Martins, L.; Pulcinelli, S.H.; Santilli, C.V.; Briois, V. Operando XAS/Raman/MS monitoring of ethanol steam reforming reaction–regeneration cycles. *Catal. Sci. Technol.* **2018**, *8*, 6297–6301. https://doi.org/10.1039/C8CY01596A.
42. Espinal, R.; Taboada, E.; Molins, E.; Chimentao, R.J.; Medina, F.; Llorca, J. Cobalt hydrotalcites as catalysts for bioethanol steam reforming. The promoting effect of potassium on catalyst activity and long-term stability. *Appl. Catal. B Environ.* **2012**, *127*, 59–67. https://doi.org/10.1016/j.apcatb.2012.08.006.
43. Espinal, R.; Taboada, E.; Molins, E.; Chimentao, R.J.; Medina, F.; Llorca, J. Cobalt hydrotalcite for the steam reforming of ethanol with scarce carbon production. *RSC Adv.* **2012**, *2*, 2946–2956. https://doi.org/10.1039/C2RA00936F.
44. Huck-Iriart, C.; Soler, L.; Casanovas, A.; Marini, C.; Prat, J.; Llorca, J.; Escudero, C. Unraveling the Chemical State of Cobalt in Co-Based Catalysts during Ethanol Steam Reforming: An in Situ Study by Near Ambient Pressure XPS and XANES. *ACS Catal.* **2018**, *8*, 9625–9636. https://doi.org/10.1021/acscatal.8b02666.
45. Li, M.R.; Wang, G.C. The mechanism of ethanol steam reforming on the Co^0 and Co^{2+} sites: A DFT study. *J. Catal.* **2018**, *365*, 391–404. https://doi.org/10.1016/j.jcat.2018.07.002.
46. Li, X.; Zheng, Z.; Wang, S.; Sun, C.; Dai, R.; Wu, Xu.; An, X.; Xie, X. Preparation Characterization of Core-Shell Composite Zeolite, B.E.A.@.M.F.I.; Their Catalytic Properties in, E.S.R. *Catal. Lett.* **2019**, *149*, 766–777. https://doi.org/10.1007/s10562-018-2638-3.
47. Sekine, Y.; Nakazawa, Y.; Oyama, K.; Shimizu, T.; Ogo, S. Effect of small amount of Fe addition on ethanol steam reforming over Co/Al_2O_3 catalyst. *Appl. Catal. A Gen.* **2014**, *472*, 113–122. https://doi.org/10.1016/j.apcata.2013.11.026.
48. Chen, C.C.; Tseng, H.H.; Lin, Y.L.; Chen, W.H. Hydrogen production and carbon dioxide enrichment from ethanol steam reforming followed by water gas shift reaction. *J. Clean. Prod.* **2017**, *162*, 1430–1441. https://doi.org/10.1016/j.jclepro.2017.06.149.
49. Cheng, F.; Dupont, V. Steam Reforming of Bio-Compounds with Auto-Reduced Nickel Catalyst. *Catalysts* **2017**, *7*, 114. https://doi.org/ 10.3390/catal7040114.
50. Cheng, F.; Dupont, V.; Twigg, M.V. Direct reduction of nickel catalyst with model bio-compounds. *Appl. Catal. B Environ.* **2017**, *200*, 121–132. https://doi.org/10.1016/j.apcatb.2016.06.044.
51. He, L.; Hu, S.; Jiang, L.; Liao, G.; Zhang, L.; Han, H.; Chen, X.; Wang, Y.; Xu, K.; Su, Sheng.; Xiang, J. Co-production of hydrogen and carbon nanotubes from the decomposition/reforming of biomass-derived organics over $Ni/\alpha\text{-}Al_2O_3$ catalyst: Performance of different compounds. *Fuel* **2017**, *210*, 307–314. https://doi.org/10.1016/j.fuel.2017.08.080.
52. Contreras, J.L.; Salmones, J.; Colín-Luna, J.A.; Nuño, L.; Quintana, B.; Córdova, I.; Zeifert, B.; Tapia, C.; Fuentes, G.A.

Catalysts for H_2 production using the ethanol steam reforming (a review). *Int. J. Hydrogen Energy* **2014**, *39*, 18835–18853. https://doi.org/10.1016/j.ijhydene.2014.08.072.

53. Zanchet, D.; Santos, J.B.O.; Damyanova, S.; Gallo, J.M.R.; Bueno, J.M.C. Toward Understanding Metal-Catalyzed Ethanol Reforming. *ACS Catal.* **2015**, *5*, 3841–3863. https://doi.org/10.1021/cs5020755.
54. Hou, T.; Zhang, S.; Chen, Y.; Wang, D.; Cai, W. Hydrogen production from ethanol reforming: Catalysts and reaction mechanism. *Renew. Sustain. Energy Rev.* **2015**, *44*, 132–148. https://doi.org/10.1016/j.rser.2014.12.023.
55. *Aspen Plus*, version 11; Aspen Tech: Bedford, MA, USA, 2019..
56. Everaert, K.; Baeyens, J. Catalytic combustion of volatile organic compounds. *J. Hazard. Mater.* **2004**, *109*, 113–139. https://doi.org/10.1016/j.jhazmat.2004.03.019.
57. Butcher, J. Runge-kutta methods. *Scholarpedia* **2007**, *2*, 3147.
58. Nauman, E.B. *Chemical Reactor Design, Optimization, and Scaleup*; AIChE: New York, NY, USA, 2008.
59. Musa, H.; Ibrahim, S.; Waziri, M.Y. A simplified derivation and analysis of fourth order Runge Kutta method. *Int. J. Comput. Appl.* **2010**, *9*, 51–55. https://doi.org/10.5120/1402-1891.
60. Deng, Y.; Li, S.; Liu, H.; Zhang, H.; Baeyens, J. Recent Research in Solar-Driven Hydrogen Production. *Sustainability* **2024**, *16*, 2883. https://doi.org/10.3390/su16072883.
61. Silva, G.H.R.D.; Nascimento, A.; Baum, C.D.; Nascimento, N.; Mathias, M.H.; Amro, M. Renewable energy perspectives: Brazilian case study on green hydrogen production. *AIMS Energy* **2025**, *13*, 449–470. https://doi.org/10.3934/energy.2025017.
62. Wu, Y.; Su, C.; Liao, Z.; Zhang, G.; Jiang, Y.; Wang, Y.; Zhang, C.; Cai, D.; Qin, P.; Tan, T. Sequential catalytic lignin valorization and bioethanol production: An integrated biorefinery strategy. *Biotechnol Biofuels* **2024**, *17*, 8. https://doi.org/10.1186/s13068-024-02459-8.
63. Riani, P.; Garbarino, G.; Canepa, F.; Guido, B. Cobalt nanoparticles mechanically deposited on α-Al_2O_3: A competitive catalyst for the production of hydrogen through ethanol steam reforming. *J. Chem. Technol. Biotechnol.* **2019**, *94*, 538–546. https://doi.org/10.1002/jctb.5800.
64. Han, S.J.; Song, J.W.; Yoo, J.; Park, S.; Kang, K.H.; Song, I.K. Sorption-enhanced hydrogen production by steam reforming of ethanol over mesoporous Co/$CaOAl_2O_3$ xerogel catalysts: Effect of Ca/Al molar ratio. *Int. J. Hydrogen Energy* **2017**, *42*, 5886–5898. https://doi.org/10.1016/j.ijhydene.2016.12.075.
65. Dobosz, J.; Małecka, M.; Zawadzki, M. Hydrogen generation via ethanol steam reforming over Co/HAp catalysts. *J. Energy Inst.* **2018**, *91*, 411–423. https://doi.org/10.1016/j.joei.2017.02.001.
66. Rodriguez-Gomez, A.; Holgado, J.P.; Caballero, A. Cobalt Carbide Identified as Catalytic Site for the Dehydrogenation of Ethanol to Acetaldehyde. *ACS Catal.* **2017**, *7*, 5243–5247. https://doi.org/10.1021/acscatal.7b01348.
67. Ohno, T.; Ochibe, S.; Wachi, H.; Hirai, H.; Arai, T.; Sakamoto, N.; Suzuki, H.; Matsuda, T. Preparation of metal catalyst component doped perovskite catalyst particle for steam reforming process by chemical solution deposition with partial reduction. *Adv. Powder Technol.* **2018**, *29*, 584–589. https://doi.org/10.1016/j.apt.2017.11.030.
68. Greluk, M.; Rotko, M.; Słowik, G.; Turczyniak-Surdacka, S. Hydrogen production by steam reforming of ethanol over Co/CeO_2 catalysts: Effect of cobalt content. *J. Energy Inst.* **2019**, *92*, 222–238. https://doi.org/10.1016/j.joei.2018.01.013.
69. Gac, W.; Greluk, M.; Słowik, G.; Turczyniak-Surdacka, S. Structural and surface changes of cobalt modified manganese oxide during activation and ethanol steam reforming reaction. *Appl. Surf. Sci.* **2018**, *440*, 1047–1062. https://doi.org/10.1016/j.apsusc.2018.01.242.
70. Rodriguez-Gomez, A.; Caballero, A. Bimetallic Ni-Co/SBA-15 catalysts for reforming of ethanol: How cobalt modifies the nickel metal phase and product distribution. *Mol. Catal.* **2018**, *449*, 122–130. https://doi.org/10.1016/j.mcat.2018.02.011.
71. Słowik, G.; Greluk, M.; Rotko, M.; Machocki, A. Evolution of the structure of unpromoted and potassium-promoted ceria-supported nickel catalysts in the steam reforming of ethanol. *Appl. Catal. B: Environ.* **2018**, *221*, 490–509. https://doi.org/10.1016/j.apcatb.2017.09.052.
72. Pinton, N.; Vidal, M.V.; Signoretto, M.; Martínez-Arias, A.; Cortés Corberán, V. Ethanol steam reforming on nanostructured catalysts of Ni, Co and CeO_2: Influence of synthesis method on activity, deactivation and regenerability. *Catal. Today* **2017**, *296*, 135–143. https://doi.org/10.1016/j.cattod.2017.06.022.
73. Garbarino, G.; Cavattoni, T.; Riani, P.; Brescia, R.; Canepa, F.; Busca, G. On the Role of Support in Metallic Heterogeneous Catalysis: A Study of Unsupported Nickel–Cobalt Alloy Nanoparticles in Ethanol Steam Reforming. *Catal. Lett.* **2019**, *149*, 929–941. https://doi.org/10.1007/s10562-019-02688-9.
74. Shejale, A.D.; Yadav, G.D. Cu promoted Ni-Co/hydrotalcite catalyst for improved hydrogen production in comparison with several modified Ni-based catalysts via steam reforming of ethanol. *Int. J. Hydrogen Energy* **2017**, *42*, 11321–11332. https://doi.org/10.1016/j.ijhydene.2017.03.052.
75. Ángel-Soto, J.; Martínez-Rosales, M.; Ángel-Soto, P.; Zamorategui-Molina, A. Synthesis, characterization and catalytic application of Ni catalysts supported on alumina-zirconia mixed oxides. *Bull. Mater. Sci.* **2017**, *40*, 1309–1318. https://doi.org/10.1007/s12034-017-1493-y.
76. Menegazzo, F.; Pizzolitto, C.; Zanardo, D.; Signoretto, M.; Buysschaert, C.; Bény, G.; Di Michele, A. Hydrogen

Production by Ethanol Steam Reforming on Ni-Based Catalysts: Effect of the Support and of CaO and Au Doping. *ChemistrySelect* **2017**, *2*, 9523–9531. https://doi.org/10.1002/slct.201702053.

77. Gac, W.; Greluk,M.; Słowik, G.; Millot, Y.; Valentin, L.; Dzwigaj, S. Effects of dealumination on the performance of Ni-containing BEA catalysts in bioethanol steam reforming. *Appl. Catal. B Environ.* **2018**, *237*, 94–109. https://doi.org/10.1016/j.apcatb.2018.05.040.
78. Wang, S.; He, B.; Tian, R.; Sun, C.; Dai, R.; Li, X.; Wu, X.; An, X.; Xie, X. Ni-hierarchical Beta zeolite catalysts were applied to ethanol steam reforming: Effect of sol gel method on loading Ni and the role of hierarchical structure. *Mol. Catal.* **2018**, *453*, 64–73. https://doi.org/10.1016/j.mcat.2018.04.034.
79. Wang, M.; Kim, S.Y.; Jamsaz, A.; Pham-Ngoc, N.; Men, Y.; Jeong, D.H.; Shin, E.W. Metal-support interactions over Ni/CeO_2-ZrO_2 catalysts for ethanol steam reforming and their effects on the coke gasification. *Catal. Today* **2024**, *425*, 114341. https://doi.org/10.1016/j.cattod.2023.114341.
80. Hu, Y.; He, W.; Shen, Y. Hydrogen production from ethanol by steam reforming with recyclable $NiCaO_x$/NaCl catalysts. *Catal. Sci. Technol.* **2024**, *14*, 1062–1071. https://doi.org/10.1039/D3CY01701J.
81. Afolabi, A.T.F.; Kechagiopoulos, P.N.; Liu, Y.; Li, C.Z. Kinetic features of ethanol steam reforming and decomposition using a biochar-supported Ni catalyst. *Fuel Process. Technol.* **2021**, *212*, 106622. https://doi.org/10.1016/j.fuproc.2020.106622.
82. Xiao, Z.; Wu, C.; Wang, L.; Xu, J.; Zheng, Q.; Pan, L.; Zou, J.; Zhang, X.; Li, G. Boosting hydrogen production from steam reforming of ethanol on nickel by lanthanum doped ceria. *Appl. Catal. B Environ.* **2021**, *286*, 119884. https://doi.org/10.1016/j.apcatb.2021.119884.
83. Suriya, P.; Xu, S.; Ding, S.; Chansai, S.; Jiao, Y.; Hurd, J.; Lee, D.; Zhang, Y.; Hardacre, C.; Reubrocharoen, P.; et al. Ethanol steam reforming over Ni/ZSM-5 nanosheet for hydrogen production. *Chin. J. Chem. Eng.* **2024**, *67*, 247–256. https://doi.org/10.1016/j.cjche.2023.12.006.
84. Wang, S.; He, B.; Wang, Y.; Wu, X.; Duan, H.; Di, J.; Yu, Z.; Liu, Y.; Xin, Z.; Jia, L.; et al. Hydrogen production from the steam reforming of bioethanol over novel supported Ca/Ni-hierarchical Beta zeolite catalysts. *Int. J. Hydrogen Energy* **2021**, *46*, 36245–36256. https://doi.org/10.1016/j.ijhydene.2021.08.170.
85. Chagas, C.A.; Manfro, R.L.; Toniolo, F.S. Production of Hydrogen by Steam Reforming of Ethanol over Pd-Promoted Ni/SiO2 Catalyst. *Catal. Lett.* **2020**, *150*, 3424–3436. https://doi.org/10.1007/s10562-020-03257-1.
86. Boudadi, K.; Bellifa, A.; Márquez-Álvarez, C.; Corberán, V.C. Nickel catalysts promoted with lanthanum for ethanol steam reforming: Influence of support and treatment on activity. *Appl. Catal. A Gen.* **2021**, *619*, 118141. https://doi.org/10.1016/j.apcata.2021.118141.
87. Pizzolitto, C.; Menegazzo, F.; Ghedini, E.; Innocenti, G.; Michele, A.D.; Mattarelli, M.; Cruciani, G.; Cavani, F.; Signoretto, M. Ethanol Steam Reforming on Lanthanum Ni-ZrO2 Catalysts. *ACS Sustain. Chem. Eng.* **2020**, *8*, 10756–10766. https://doi.org/10.1021/acssuschemeng.0c02373.
88. Choong, C.K.S.; Du, Y.; Poh, C.K.; Ong, S.W.D.; Chen, L.; Borgna, A. Structural understanding of IrFe catalyst for renewable hydrogen production from ethanol steam reforming. *Appl. Catal. B Environ. Energy* **2024**, *345*, 123630. https://doi.org/10.1016/j.apcatb.2023.123630.
89. Bkangmo Kontchouo, F.M.; Shao, Y.; Zhang, S.; Gholizadeh, M.; Hu, X. Steam reforming of ethanol, acetaldehyde, acetone and acetic acid: Understanding the reaction intermediates and nature of coke. *Chem. Eng. Sci.* **2023**, *265*, 118257. https://doi.org/10.1016/j.ces.2022.118257.
90. Wang, Y.; Zhou, Hui.; Yao, D.; Olguin, G.; Ding, H.; Qu, B.; Xie, W.; Fu, Z.; Guo, Y.; Wang, X.; Li, A.; et al. Ni-CaO-$CaZrO_3$ bi-functional materials for high purity hydrogen production via sorption enhanced steam reforming of ethanol. *J. Clean. Prod.* **2024**, *446*, 141397. https://doi.org/10.1016/j.jclepro.2024.141397.
91. Liu, H.; Ding, R.; Zhang, Y.; Li, H.; Li, S. Magnesium promoted hydrocalumite derived nickel catalysts for ethanol steam reforming. *Int. J. Hydrogen Energy* **2023**, *48*, 13804–13813. https://doi.org/10.1016/j.ijhydene.2022.12.295.
92. Greluk, M.; Gac, W.; Rotko, M.; Słowik, G.; Turczyniak-Surdacka, S. Co/CeO_2 and Ni/CeO_2 catalysts for ethanol steam reforming: Effect of the cobalt/nickel dispersion on catalysts properties. *J. Catal.* **2021**, *393*, 159–178. https://doi.org/10.1016/j.jcat.2020.11.009.
93. Li, R.; Liu, C.; Li, L.; Xu, J.; Ma, J.; Ni, J.; Yan, J.; Han, J.; Pan, Y.; Liu, Y.; et al. Regulating cobalt chemical state by CeO_2 facets preferred exposure for improved ethanol steam reforming. *Fuel* **2023**, *336*, 126758. https://doi.org/10.1016/j.fuel.2022.126758.
94. Da Costa-Serra, J.F.; Miralles-Martínez, A.; García-Muñoz, B.; Maestro-Cuadrado, S.; Chica, A. Ni and Co-based catalysts supported on ITQ-6 zeolite for hydrogen production by steam reforming of ethanol. *Int. J. Hydrogen Energy* **2023**, *48*, 26518–26525. https://doi.org/10.1016/j.ijhydene.2022.11.128.
95. Liu, H.; Li, H.; Li, S. Ni-hydrocalumite derived catalysts for ethanol steam reforming on hydrogen production. *Int. J. Hydrogen Energy* **2022**, *47*, 24610–24618. https://doi.org/10.1016/j.ijhydene.2021.07.141.
96. Razavian, M.; Fatemi, S.; Malek mohammadi, M.; Nouralishahi, A. Nickel supported ZIF-8.PEG modified catalyst: A designed active catalyst with high H_2 productivity in steam reforming of ethanol at moderate temperature. *J. Environ.*

Chem. Eng. **2021**, *9*, 105531. https://doi.org/10.1016/j.jece.2021.105531.

97. Shen, Q.; Jiang, Y.; Li, S.; Yang, G.; Zhang, H.; Zhang, Z.; Pan, X. Hydrogen production by ethanol steam reforming over Ni-doped $LaNiXCo_{1-x}O_{3-\delta}$ perovskites prepared by EDTA-citric acid sol–gel method. *J. Sol-Gel Sci. Technol.* **2021**, *99*, 420–429. https://doi.org/10.1007/s10971-021-05588-w.
98. Zhang, C.; Wen, H.; Chen, C.; Cai, D.; Fu, C.; Li, P.; Qin, P.; Tan, T. Simultaneous saccharification and juice co-fermentation for high-titer ethanol production using sweet sorghum stalk. *Renewable Energy* **2019**, *134*, 44–53. https://doi.org/10.1016/j.renene.2018.11.005.
99. Hosseinaei, O.; Wang, S.; Enayati, A.A.; Rials, T.G. Effects of hemicellulose extraction on properties of wood flour and wood–plastic composites. *Compos. Part A* **2012**, *43*, 686–694. https://doi.org/10.1016/j.compositesa.2012.01.007.
100. Bizzo, W.A.; Lenco, P.C.; Carvalho, D.J.; Veiga, J.P.S. The generation of residual biomass during the production of bio-ethanol from sugarcane, its characterization and its use in energy production. *Renew. Sustain. Energy Rev.* **2014**, *29*, 589–603. https://doi.org/10.1016/j.rser.2013.08.056.
101. Chiesa, S.; Gnansounou, E. Protein extraction from biomass in a bioethanol refinery—Possible dietary applications: Use as animal feed and potential extension to human consumption. *Bioresourse Technol.* **2011**, *102*, 427–436. https://doi.org/10.1016/j.biortech.2010.07.125.
102. Su, C.; Zhang, C.; Wu, Y.; Zhu, Q.; Wen, J.; Wang, Y.; Zhao, J.; Liu, Y.; Qin, P.; Cai, D. Combination of pH adjusting and intermittent feeding can improve fermentative acetone-butanol-ethanol (ABE) production from steam exploded corn stover. *Renew. Energy* **2022**, *200*, 592–600. https://doi.org/10.1016/j.renene.2022.10.008.
103. Yu, Y.; Wu, J.; Ren, X.; Lau, A.; Rezaei, H.; Takada, M.; Bi, X.; Sokhansanj, S. Steam explosion of lignocellulosic biomass for multiple advanced bioenergy processes: A review. *Renew. Sustain. Energy Rev.* **2022**, *154*, 111871. https://doi.org/10.1016/j.rser.2021.111871.
104. Li, B.; Liu, N.; Zhao, X. Response mechanisms of Saccharomyces cerevisiae to the stress factors present in lignocellulose hydrolysate and strategies for constructing robust strains. *Biotechnol. Biofuels Bioprod.* **2022**, *15*, 28. https://doi.org/10.1186/s13068-022-02127-9.
105. Wu, Y.; Su, C.; Zhang, G.; Liao, Z.; Wen, J.; Wang, Y.; Jiang, Y.; Zhang, C.; Cai, D. High-Titer Bioethanol Production from Steam-Exploded Corn Stover Using an Engineering Saccharomyces cerevisiae Strain with High Inhibitor Tolerance. *Fermentation* **2023**, *9*, 906. https://doi.org/10.3390/fermentation9100906.